



Non-uniform illumination in low concentration photovoltaic systems based on small-scale linear Fresnel reflectors



A. Barbón ^a, P. Fortuny Ayuso ^b, L. Bayón ^{b,*}, J.A. Fernández-Rubiera ^a

^a Department of Electrical Engineering, University of Oviedo, Spain

^b Department of Mathematics, University of Oviedo, Spain

ARTICLE INFO

Article history:

Received 21 May 2021

Received in revised form

2 September 2021

Accepted 27 September 2021

Available online 30 September 2021

Keywords:

Low concentration photovoltaic systems

Small-scale linear Fresnel reflectors

Non-uniform illumination

Hot-spot

ABSTRACT

Low concentration photovoltaic systems improve performance by absorbing and concentrating more sunlight than non-concentration ones. However, they require uniform illumination of the PV cells, as their electrical performance can decrease dramatically otherwise. A thorough analysis of the design causes of non-uniform illumination in small-scale linear Fresnel reflectors (SSLFR) is carried out, yielding the main parameters to be optimized. Then, such an optimized SSLFR guaranteeing uniform illumination is designed, and an optimum operation interval is estimated during which, furthermore, neither shading nor blocking on the mirrors happens. The study requires computing the maximum optimal transverse incidence angle, θ_{t_0} , whose influence on the time-span of optimum operation, width of the SSLFR, annual solar irradiation, width of the mirrors, and position of the mirrors is also studied. We include a detailed example showing the accuracy of our calculations, using Monte Carlo Ray Tracing.

© 2021 Elsevier Ltd. All rights reserved.

1. Introduction

Photovoltaic (PV) systems are one of the main applications of solar energy, and apart from their intrinsic benefits, they have some specific advantages: freedom of installation, multiple applications, and commercial availability [1]. It is estimated [2] that PV energy generation by 2050 may reach 14.5% from residential roof installations, 11.5% from non-residential roof installations and 21.4% from (solar) power plants. The leveled cost of energy (LCOE), moreover, is expected to decrease from 0.085 (USD/kWh) to between 0.014 and 0.05 (USD/kWh) by 2050 [3].

A typical application of PV technology are Concentrated Photovoltaic Systems (CPV), with high conversion efficiency, low cost, and which can provide electric and thermal energy at the same time. Their main drawback is that concentrating the solar irradiance may make its distribution non-uniform on the PV cells, causing efficiency losses.

The geometric concentration ratio (the area of the primary lens or mirror divided by that of the PV cells) divides CPVs into three main groups: low, medium and high concentration [4]. The first are called Low Concentration PV systems (LCPVs) have geometric

concentration ratio between 2 and 10 suns [5], and in them conventional high-performance silicon PV cells designed for 1 sun are used [6]. The efficiency of LCPVs depends strongly on that of the PV cells, which require uniform illumination on their whole surface for their correct operation. This is one of the key constraints in the design of any LCPV.

In this study we focus on the design of an LCPV using a Small Scale Linear Fresnel Reflector (SSLFR). These reflectors concentrate sunlight onto the secondary system using a row of longitudinal mirrors, and have been thoroughly studied (see Refs. [7–9], [10], for instance). In Refs. [7,10] different compact versions are presented, and optical designs and analyses are carried out, using statistical simulation techniques (Monte Carlo Ray Tracing). In Ref. [9], a hybrid concentrating PV/Thermal system with beam splitter and fully tracked linear Fresnel reflector is proposed, and its structural parameters are computed and optimized.

The general structure of an SSLFR is a series of rows of parallel mirrors (the primary reflector system) placed on a mobile structure. The mirrors reflect the incident solar irradiance towards a surface (usually with a secondary reflector system) on a fixed structure. They are simple and inexpensive [11] but their efficiency is highly dependent on the incidence angle.

In our application of SSLFRs to LCPV technology, we are going to focus on the issue of uniform illumination of the PV cells, as this is the most important property to guarantee: non-uniform

* Corresponding author.

E-mail address: bayon@uniovi.es (L. Bayón).

illumination causes higher than expected Ohmic drops [12], mismatch between series-connected PV cells, and Hot-spots [13].

Hot-spots are due to an heterogeneous distribution of the solar irradiance on the PV cells —their name comes from the increase of temperature in the corresponding area of the cell. There is a direct correlation between the existence of hot spots and faults in PV modules [14], which has led to the modeling of the effects of non-uniform solar irradiance of PV cells [15], the optimization of their distribution [16], the attempt to balance the high concentration and the uniformity of the distribution of solar irradiance [17], and the effect of this non-uniform distribution on multi-junction PV cells, among other studies. In summary, the design of an SSLFR for PV applications must guarantee the total absence of hot-spots. Our aim in this paper is precisely to present a design which yields *uniform* distribution of the solar irradiance on the PV cells during the operation time of the system.

It is difficult to exactly reproduce (either experimentally or numerically) a non-uniform illumination caused by a real solar concentrator [18], and Monte-Carlo ray tracing is usually employed [19], which reduces simulation time and data volume [5]. We use this technique in the simulations presented to validate our results, using SolTrace© [20], commonly used for PV systems [19].

An important parameter in our design is the transverse solar angle at time t , θ_t , which, apart from being relevant to the uniform illumination, influences the possible existence of blocking and shading between the mirrors. This angle is usually projected in the transverse and longitudinal planes. We carry out the transverse study, as the other one has already been covered elsewhere [21,22]. An analysis of the influence of θ_t on the received irradiation is also done. In the end, two main and antithetical parameters influence the design: the total energy received by the cells and the size of the system, and a compromise has to be reached between the two. Once a specific design is chosen, we study several issues related to the behavior of the SSLFR – PV system in motion, and check the amount of shading taking place when the system works out of its design conditions.

The paper is organized as follows. Section 2 summarizes the main components of an SSLFR used in a low concentrated photovoltaic system. The causes of non-uniform illumination in LCPVs based on SSLFRs are presented in Section 3. Section 4 studies the main properties dealing with the optimization of the design. The behavior of the SSLFR in motion is covered in Section 5. Numerical simulations and verifications are presented in Section 6 and, finally, Section 7 summarizes the main contributions and conclusions of the paper.

2. Background

2.1. Constructive aspects of an SSLFR

The diagram in Fig. 1 enumerates the systems that configure a conventional SSLFR [11] for use in domestic water heating [23], heating/cooling of living space [24], etc. We aim to redesign it for PV generation.

Roughly (see Fig. 1), an SSLFR is composed of two main parts: the primary reflector system (containing the row of parallel mirrors and the several tracking elements) and the secondary reflector system (which itself contains the absorber tube, receiver cavity, insulation, and glass cover), lying on the focal line of the Fresnel mirrors. The primary reflector system is mounted on a mobile structure. The secondary reflector system is mounted on a fixed structure, located at a specific height above the primary reflector system.

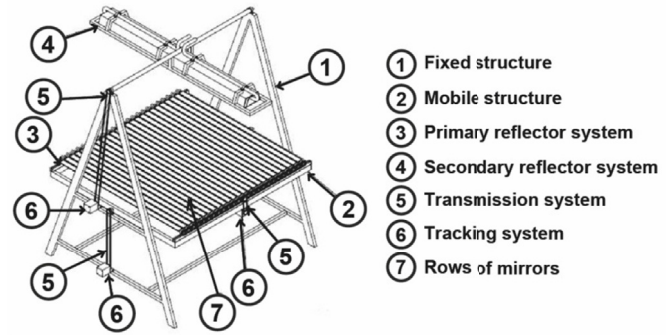


Fig. 1. Scheme of an SSLFR.

2.2. Relevant parameters

There are $2n + 1$ mirrors in the primary reflector system: the central one ($i = 0$), n to its left, and n to its right. The system, except for the orientation of the mirrors at time t , is totally symmetric with respect to the vertical axis joining the focal point O (the center of the secondary system) and the midpoint of the central mirror. The system is designed such that performance is also symmetrical throughout the day.

At this point, we want to compute the optimum position of the primary mirrors. Specifically, we wish to optimize:

1. The number n of mirrors on each side of the central mirror.
2. The distance $L_i > 0$ from the midpoint of each mirror to the midpoint of the central mirror (from which the distance $d_i > 0$ between mirrors i and $i + 1$ can be computed).
3. The width W_{Mi} of each mirror (which depend on i).

From L_i and W_{Mi} one can compute d_i , the distance between mirrors, as seen in Fig. 2.

The third item above (the width) is a novelty with respect to previous studies performed by the authors, where the SSLFR had an absorber tube in which a fluid was moving, instead of a string of PV cells. In those systems (see, v.gr [21]), the mirrors were all equal in order to simplify the design, as hot spots were irrelevant. However, in our present system, they impose an important constraint: it is paramount that all the PV cells be illuminated equally over all their

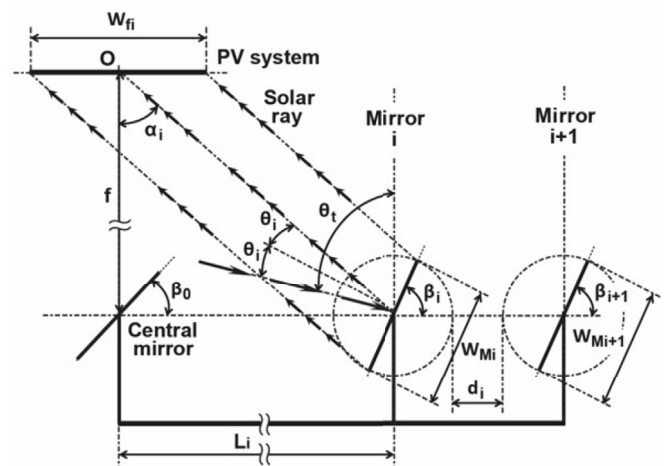


Fig. 2. Basic definitions of the SSLFR.

surface (same flux density everywhere) during the operation time. This imposes several conditions.

An SSLFR can have three rotating parts: the mobile structure, and the secondary reflector system may be rotated on the East-West axis; and the rows of mirrors can be rotated on the North-South axis following the Sun's daily movement (see Figs. 3 and 4). In this paper, only the motion of the mirrors is of interest, and to study this, we only need to consider the central mirror, and all of them rotate at the same angular speed. Obviously, the tilt of each mirror must be such that the incident ray on the midpoint (arriving with angle θ_t) reaches the focal line after the reflection. In order to control the tilt of all the mirrors, one only needs to position all of

them correctly at the start of the day and move them synchronously [26] with the Sun angle:

$$\theta_t = \arctan\left(\frac{\sin \gamma_S}{\tan \alpha_S}\right) \quad (1)$$

where α_S is the solar altitude and γ_S is the solar azimuth, both of which depend on the declination δ , latitude λ and hour angle ω . Formulas for computing these values are easily found (e.g. Ref. [25]). Our sign convention is: $\theta_t < 0$ before noon and $\theta_t > 0$ after noon. Finally, for each location, θ_t depends only on the day of the year N and the solar time T :

$$\theta_t = F(N, T) \quad (2)$$

Our optimization method starts by setting the worst working conditions: the worst values of θ_t , which we call θ_{t_0} (i.e. the worst times of the day, symmetrical around noon) and the "worst mirror", which is the one farthest from the Sun at t_0 . Any distance between mirrors which guarantees the absence of shading and blocking for this worst mirror and its adjacent at this worst time, also guarantees their absence at any other moment between any other two consecutive mirrors, during the operation time. That is, we are designing our SSLFR so that it works optimally during the operation interval (in transverse sun angles):

$$\theta_t \in [-\theta_{t_0}, \theta_{t_0}] \quad (3)$$

A correct choice of θ_{t_0} is key in our design, as it will influence other important parameters like the total width of the system, the ratio of yearly solar irradiance sent to the PV cells, or the daily time span without shading or blocking. We need some preliminary definitions.

The angle between the vertical axis and the line joining the center of mirror i with the focal point O is called α_i and its value is:

$$\alpha_i = \arctan\frac{L_i}{f}; \quad 1 \leq i \leq n \quad (4)$$

both on the left and on the right sides, with $L_0 = 0$ for the central mirror. (From now on, any value with an index i depends on mirror i).

The angle which mirror i forms with the horizontal is called its tilt: β_i . It obviously depends on θ_t , as the Sun ray meeting the midpoint of mirror i must be reflected towards O . This gives:

$$\beta_i = \frac{-\theta_t \pm \alpha_i}{2}; \quad 1 \leq i \leq n \quad (5)$$

where \pm stands for: $-$ for mirrors on the left side and $+$ otherwise. Notice that for $i = 0$, $\alpha_0 = 0$ and then $\beta_0 = \theta_t/2$ at all times. By convention, $\beta_i > 0$ when measured counter-clockwise above the horizontal. Notice that the focal plane is located at a distance f from the reflecting element placed in the center of the SSLFR ($L_0 = 0$). The pivoting point of each mirror coincides with its midpoint, so that the mirror is always focused on O .

2.3. The secondary system

In our design, the secondary system does not include a reflector. It consists of the PV cells, the active cooling system, the isolation material and the protective casing, secondary structure, and the shaft (Fig. 5). The cells are the smallest element of the PV system, there being several of them interconnected and encapsulated. Most of the solar irradiance absorbed by them is converted into heat, which is mostly absorbed by the cooling system (otherwise the cells either malfunction or work very inefficiently). The parameters

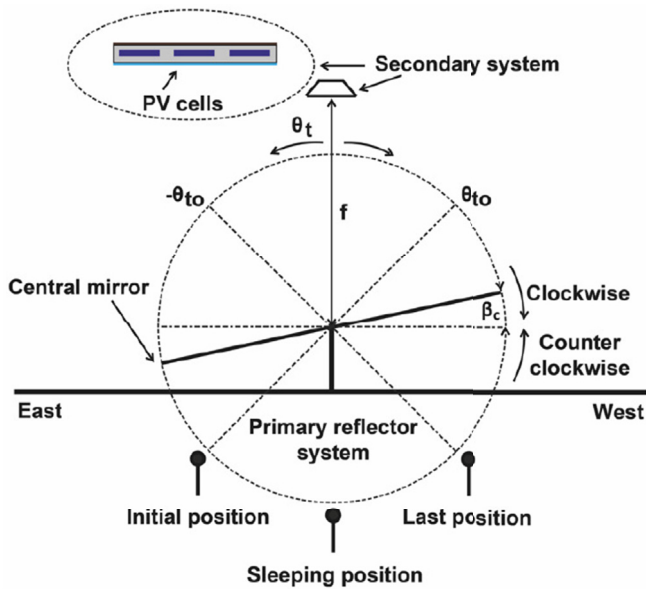


Fig. 3. Mirrors movement.

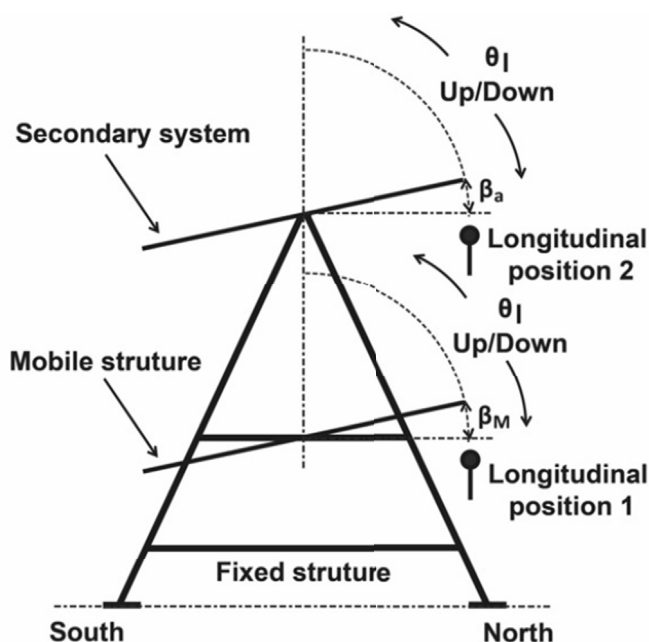


Fig. 4. Mobile structure and secondary system movements.

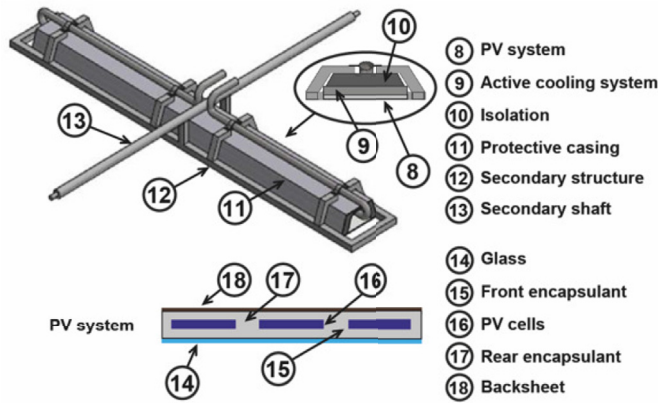


Fig. 5. Secondary system.

of the PV system are: W_{PV} (width), L_{PV} (length), whereas the cooling system has width W_{ACS} and length L_{ACS} (all in units of m).

2.4. Note on the transverse study

As is usual, the design considers the solar rays projected onto two reference planes [27], producing the longitudinal and transverse projections [21], ought to be studied. On one hand, we need to ensure that the PV cells receive a homogeneous distribution of irradiance during the whole operation time, in both directions. On the other, we want to guarantee that there is neither shading nor blocking of the Sun rays by the mirrors (which is a transverse property). Both studies are independent of each other [27], and we refer the reader to previous works of some of the authors [21,22].

The longitudinal solution found in those references ensures that the rays reflected by the mirrors in the that direction are perpendicular to the floor so that the PV cells are fully and homogeneously illuminated longitudinally during the whole operation time. This also causes the secondary system to have the same length as the mirrors of the primary reflector system. Finally, as both fields (primary and secondary) are centered with respect to the SSLFR center, the design is more compact. All these properties are good for our design.

3. Causes of non-uniform illumination of the PV cells

The majority of SSLFR applications are for heating, and use an absorber where our model has PV cells. This renders the uniformity of illumination mostly irrelevant [28–30]. However, for LCPVs, an heterogeneous illumination of the PV system decreases their fill factor and overall electrical efficiency [18] and may even damage the cells [14].

If we call W_{ai} the width of the PV system illuminated by the i – th mirror, then, using the notation above [30], gives:

$$W_{ai} = W_{Mi} \cdot [\cos \beta_i \pm \sin \beta_i \tan \alpha_i]; \quad 1 \leq i \leq n \tag{6}$$

Notice that, as α_i and β_i are not free variables, (6) depends essentially on W_{Mi} , d , n and f (but this last one will be considered fixed at 1.5 (m), as is usual [30–32]). Thus, W_{Mi} , d and n are the design parameters which may give rise to non-uniform illumination. We study how their influence on it in the next sections.

In the simulations of the flux distribution on the PV cells, the Monte-Carlo Ray tracing technique has been used, by means of SolTrace™ [19,20], choosing Almeria (Spain), at 36°50'07"N latitude, 02°24'08"W longitude and 22 (m) elevation, as the geographical location. Our 3D model of the SSLFR assumes all the mirrors are perfect, flat and without fabrication errors. The governing parameters of the system are given in Table 1 (and these are fixed throughout all the rest of the study). Finally, 10^7 light rays have been used for the simulation [33].

3.1. Shading and blocking contribution to non-uniformity (small d)

The spacing between consecutive mirrors determines the absence or not of both shading (i.e. one mirror creates a shadow on an adjacent one) and blocking (one mirror blocks the reflected rays from an adjacent one). In this section we show, by an example, how any of these events gives rise to non-uniform illumination of the PV cells, so that both need to be avoided.

Consider a design with $n = 2$ (i.e. 5 mirrors in total), distance between the centers of the mirrors $d = 0.05$ (m), and width $W_M = 0.30$ (m). Assume the width of the PV cells is $W_{PV} = 0.28$ (m). As elsewhere, the rest of parameters are as in Table 1. All the simulations have been carried out with SolTrace.

The simulation for this example is depicted in Fig. 6(left) for the Summer Equinox ($N = 172$) at $T = 9 : 00$, and the shading between mirrors 1 and 2 (the rightmost ones) is apparent. Fig. 6(right) shows the flux density (W/m^2) on the receiver for the same instant. The shading produces the strong lack of uniformity on the East side of the cells. There is some lesser lack of uniformity on the West side, but much less relevant.

Blocking gives rise to a completely parallel phenomenon, and we do not provide a simulation.

3.2. Separation between mirrors (large d)

As d increases, shading and blocking disappear, but an excessive value of d gives also rise to non-uniform illumination of the PV system, as our next example shows.

Consider the design proposed in Ref. [34] which avoids both shading and blocking: there are 5 mirrors (so that $n = 2$) of width 0.30 (m); the PV system has width 0.28 (m). Taking $d = 0.08, 0.10, 0.12$ and 0.14 (m), the flux density (W/m^2) on the PV cells follows the pattern shown in Fig. 7 for $N = 172, T = 9 : 00$. The non-uniformity of the illumination is noticeable, and clearly increases with d .

Table 1 Fixed parameters used in the study.

	Parameters	Value
L_M	Mirror length	2.00 (m) [30]
L_{PV}	PV system length	2.00 (m) [30]
f	Height of the receiver	1.50 (m) [31]
ρ	Mirror reflectivity	0.94 [25]
Cl_m	Mirror cleanliness	0.96 [34]
Cl_g	Glass cleanliness	0.96 [34]
τ_g	Glass transmissivity	$\tau_g = 0.87$ if $\alpha_i \leq 20^\circ$, $\tau_g = 0.85$ if $20^\circ \leq \alpha_i \leq 30^\circ$ [35]

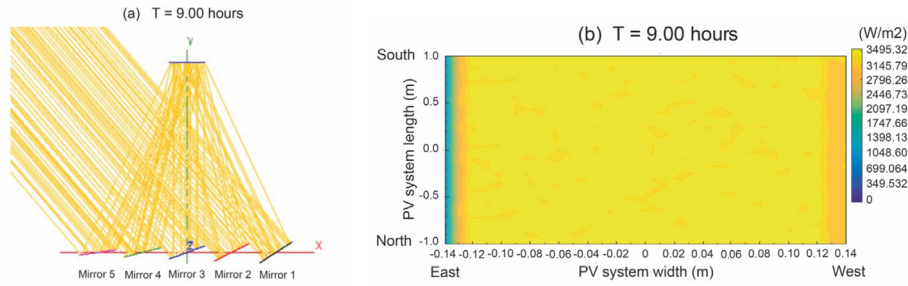


Fig. 6. Output of SolTrace for an SSLFR with shading.

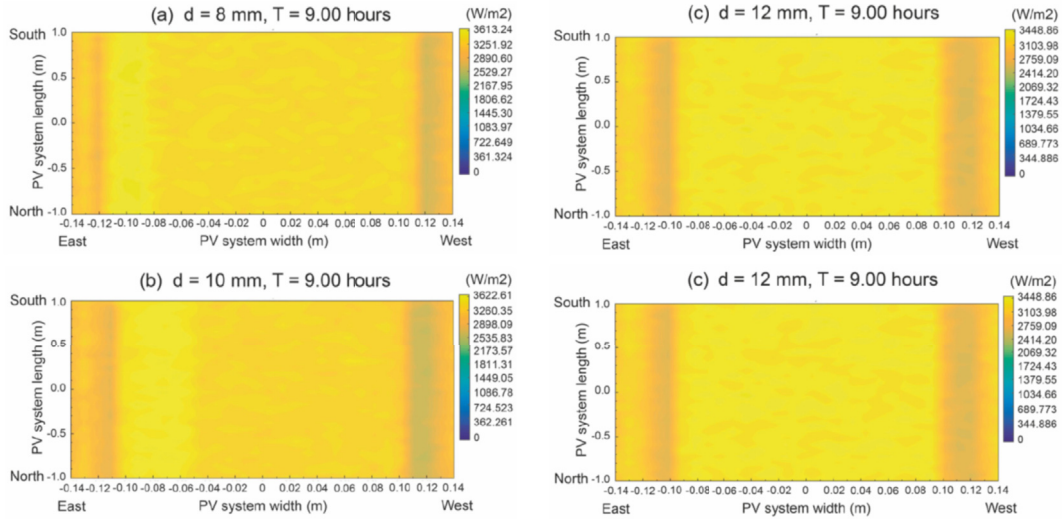


Fig. 7. SolTrace 2D view of flux density in PV cells in function of d .

3.3. Number of mirrors

The more the mirrors, the greater the probability of having a non-uniform distribution of flux on the PV system, as each mirror has a different W_{ai} . Consider a system with $n = 4$ (i.e. 9 mirrors) of width 0.16 (m). Fix a width of 0.16 (m), and $d = 0.05$ (m). The flux for $N = 172$ and $T = 9 : 00$ is pictured in Fig. 8, and is obviously non-uniform. The large difference between the W_{ai} of each mirror has a great impact on this.

3.4. Width of the PV system

The width of the PV system also bears on the uniformity (or lack thereof) of the illumination. Consider a system with $W_{PV} = 0.24$ (m) and, apart from the parameters of Table 1, set $n = 3$, each mirror of width 0.2085 (m), and $d = 0.06$ (m). The graphic in Fig. 9 evidences the (clearly) non-uniform distribution of flux on the PV system (as elsewhere, $N = 172$, $T = 9 : 00$), where the borders are practically dark, due to the wrong width of the cells.

3.5. Summary of parameters to optimize

In short, the three parameters W_{Mi} , d and n need to be optimized in order to get a uniform distribution of flux on the PV cells and prevent the problems associated to its absence.

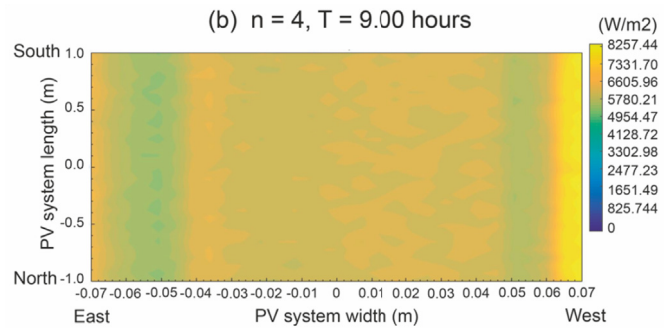


Fig. 8. SolTrace 2D view of flux density in PV cells for $n = 4$.

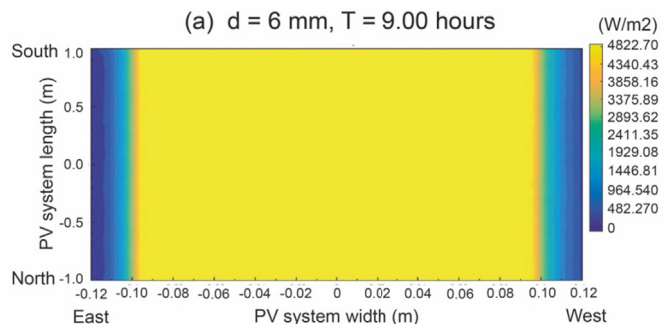


Fig. 9. SolTrace 2D view of flux density in PV cells for $n = 3$.

4. Optical design of an SSLFR with uniform illumination

Recall that our aim is to achieve a homogeneous uniform distribution of the solar irradiance reaching the PV cells during the whole operation time, and that we are only dealing with the transverse direction (see Refs. [21,22] for the longitudinal study).

We shall consider that the SSLFR is optimally designed when the following three conditions (which we will henceforward call “optimal design conditions”) hold:

- (i) There is a homogeneous flux density over all the PV cells.
- (ii) There is no shading between adjacent mirrors.
- (iii) There is no blocking between adjacent mirrors.

The first condition is the most important, whereas The other two conditions bear on the yield of the SSLFR.

For each specific day N of the year, there will be a time span $[-\theta_{t_0}, \theta_{t_0}]$, during which those three optimal design conditions hold: it will be called the optimum operation interval. At other times, only the first one will persist (as it is independent of time). Notice that shading and blocking cannot be guaranteed from sunrise to sunset for obvious geometrical reasons. Hence, the operating time is part of the design.

Thus, our design should ensure that during a specific time interval (see (32)), all the PV cells are completely illuminated by all the mirrors in a homogeneous way, without either shading or blocking. The first question, then, is: what range of operating solar incidence angles $\theta_{t_0} \in [m, M]$ should we choose in which the optimal design conditions hold? In order to know this, we need to clarify the equations which govern the system.

4.1. Main governing equations

We are going to use a modification of the method used in Ref. [21]. As it stands, mirror i can be characterized at any time by three parameters: its position (L_i), width (W_{Mi}), and tilt (β_i). We now compute the values of L_i which ensure that there is neither blocking nor shading between adjacent mirrors during the operation time. The distances d_i between consecutive centers are deduced from L_i and W_{Mi} (Fig. 2).

4.1.1. No shading

Consider the worst case (one of the two symmetrical ones): at solar time t_0 , the Sun is to the right ($\theta_{t_0} > 0$) and we look at mirrors on the left (which are the worst oriented at this time) for which $\beta_i < 0$. Fig. 10 shows the central mirror and its adjacent to the left, which are the first ones we need to consider. Obviously:

$$L_0 = 0; \beta_0 = \frac{-\theta_{t_0}}{2} \tag{7}$$

Whereas for $i = 1$, the one immediately to the left of mirror 0:

$$L_1 = A + B + C + D \\ = \frac{W_{M1}}{2} \left[\frac{-\sin \beta_1}{\cot \theta_{t_0}} + \cos \beta_1 \right] + \frac{W_{M0}}{2} \left[\frac{-\sin \beta_0}{\cot \theta_{t_0}} + \cos \beta_0 \right] \tag{8}$$

with:

$$\beta_1 = \frac{-\theta_{t_0}}{2} - \frac{1}{2} \arctan \frac{L_1}{f} \tag{9}$$

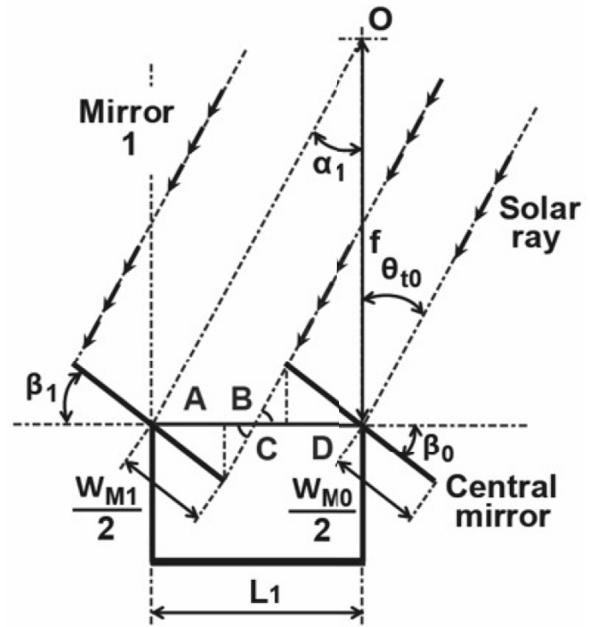


Fig. 10. Shading.

An analogous reasoning going leftwards gives the general condition:

$$L_i = L_{i-1} + \frac{W_{Mi}}{2} \left[\frac{-\sin \beta_i}{\cot \theta_{t_0}} + \cos \beta_i \right] + \frac{W_{Mi-1}}{2} \left[\frac{-\sin \beta_{i-1}}{\cot \theta_{t_0}} + \cos \beta_{i-1} \right] \tag{10}$$

with:

$$\beta_i = \frac{-\theta_{t_0}}{2} - \frac{1}{2} \arctan \frac{L_i}{f} \tag{11}$$

for $1 \leq i \leq n$, for the mirrors on the left side of the SSLFR.

As we assume the SSLFR performs symmetrically throughout the day, the values of L_i on the right side must be the same as those on the left side. Using the conventions $\theta_{t_0} < 0$, $\beta_i > 0$ for these mirrors, we obtain:

$$L_i = L_{i-1} + \frac{W_{Mi}}{2} \left[\frac{\sin \beta_i}{-\cot \theta_{t_0}} + \cos \beta_i \right] + \frac{W_{Mi-1}}{2} \left[\frac{\sin \beta_{i-1}}{-\cot \theta_{t_0}} + \cos \beta_{i-1} \right] \tag{12}$$

while, for the tilts, we get:

$$\beta_i = \frac{-\theta_{t_0}}{2} + \frac{1}{2} \arctan \frac{L_i}{f}; \quad 1 \leq i \leq n \tag{13}$$

4.1.2. No blocking

As before, we only have to reason for the positive value of θ_{t_0} and on the left side (see Fig. 11). A reasoning similar to the one carried out for shading gives, for the first two mirrors:

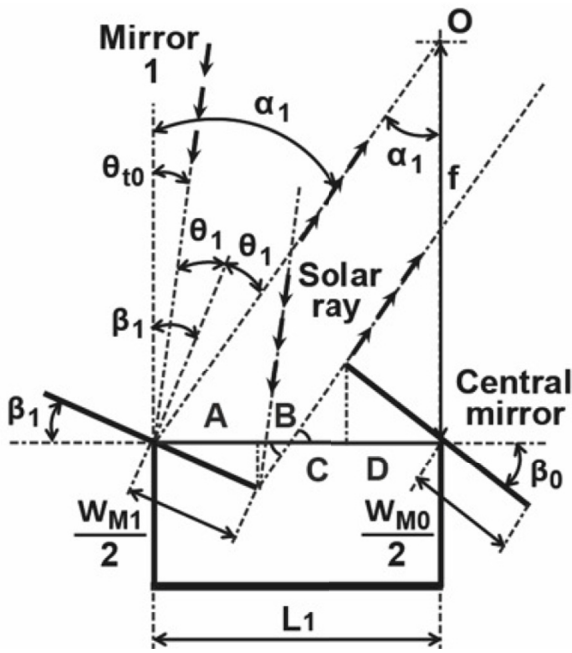


Fig. 11. Blocking.

$$L_0 = 0; \beta_0 = \frac{-\theta_{t_0}}{2} \quad (14)$$

and:

$$L_1 = A + B + C + D = \frac{W_{M1}}{2} \left[\frac{-\sin \beta_1}{\cot \alpha_1} + \cos \beta_1 \right] + \frac{W_{M0}}{2} \left[\frac{-\sin \beta_0}{\cot \alpha_1} + \cos \beta_0 \right] \quad (15)$$

with:

$$\beta_1 = \frac{-\theta_{t_0}}{2} - \frac{1}{2} \arctan \frac{L_1}{f} \quad (16)$$

In general, for $1 \leq i \leq n$, we get:

$$L_i = L_{i-1} + \frac{W_{Mi}}{2} \left[\frac{-\sin \beta_i}{\cot \alpha_i} + \cos \beta_i \right] + \frac{W_{Mi-1}}{2} \left[\frac{-\sin \beta_{i-1}}{\cot \alpha_i} + \cos \beta_{i-1} \right] \quad (17)$$

with tilts:

$$\beta_i = \frac{-\theta_{t_0}}{2} - \frac{1}{2} \arctan \frac{L_i}{f} \quad (18)$$

By symmetry, the values of L_i and β_i on the right side are:

$$L_i = L_{i-1} + \frac{W_{Mi}}{2} \left[\frac{\sin \beta_i}{\cot \alpha_i} + \cos \beta_i \right] + \frac{W_{Mi-1}}{2} \left[\frac{\sin \beta_{i-1}}{\cot \alpha_i} + \cos \beta_{i-1} \right] \quad (19)$$

and

$$\beta_i = \frac{-\theta_{t_0}}{2} + \frac{1}{2} \arctan \frac{L_i}{f} \quad (20)$$

We have verified, by means of simulations that the shading conditions (10) and (11) are more stringent than those for blocking (17) and (18).

4.1.3. Homogeneous flux density on the PV cells

As stated above, in our previous studies with thermal systems, the width of the mirrors W_{Mi} was constant and pre-defined. However, the new design using PV cells requires them to be chosen so that the flux density is guaranteed to be homogeneous during the operation time. Hence the W_{Mi} are also unknowns and have to be computed from some new conditions.

The width W_{fi} (on the secondary system, around the focal point O) illuminated by the i -th mirror is:

$$W_{fi} = W_{Mi} \cdot [\cos \beta_i \pm \sin \beta_i \tan \alpha_i]; \quad 1 \leq i \leq n \quad (21)$$

where the sign \pm is $-$ for the left side, and $+$ for the right side of the SSLFR. For $i = 0$ (central mirror), $\alpha_0 = 0$ and $\beta_0 = -\theta_{t_0}/2$. During the operation time, W_{fi} depends on the day of the year N , the solar time T and the mirror i : $W_{fi}(N, T, i)$. We fix θ_{t_0} , and the set of unknowns depending on this θ_{t_0} is: W_{Mi} , β_i and L_i .

Our requirement of uniform illumination of the PV cells is:

$$W_{fi} = W_{PV}; \quad 1 \leq i \leq n \quad (22)$$

where the width W_{PV} of the PV system is a datum. Numerical simulations show that the following property holds:

Property 1. For all days N , all values of θ_{t_0} , and for each i , the least value of $W_{fi}(N, T, i)$ (and, hence, the worst situation, as we need W_{Mi} to be such that (22) holds) happens: for the mirrors on the left side, when $T = -\theta_{t_0}$; for the mirrors on the right side, when $T = \theta_{t_0}$; the central mirror behaves symmetrically with respect to those two values.

From **Property 1**, and in order to guarantee the homogeneity of flux even at the worst situations, we solve equation (22) taking into account that now, the mirrors on the left side behave worst when the Sun is on the same side, and respectively with the right side. As the SSLFR is symmetric, we only need to solve one of the cases. We take the left one for coherence.

In summary, the following condition has to hold:

$$W_{Mi} \cdot [\cos(\beta_i + \theta_{t_0}) - \sin(\beta_i + \theta_{t_0}) \tan \alpha_i] = W_{PV}; \quad 1 \leq i \leq n \quad (23)$$

4.2. Optimum operation interval

We now provide a succinct version of the iterative optimization algorithm used for the design. Recall that we are only working with the mirrors on the left side, as the system is symmetric. The steps are the following:

1. Select a discretization of the interval $[m, M]$ to which θ_{t_0} belongs. This interval should contain the optimal design and is chosen from experience. Start with $\theta_{t_0} = m$.
2. Find the initial conditions for each mirror. For $i = 0$, we know that:

$$\beta_0 = \frac{-\theta_{t_0}}{2}; \quad L_0 = 0 \quad (24)$$

Using Equation (23), compute the width W_{M0} of the central mirror:

$$W_{M0} \cdot [\cos(\beta_0 + \theta_{t_0}) - \sin(\beta_0 + \theta_{t_0}) \tan \alpha_i] = W_{PV} \quad (25)$$

3. Solve the system of 3 equations (10), (11) and (23) (the worst conditions for the design):

$$\beta_i = \frac{-\theta_{t_0}}{2} - \frac{1}{2} \arctan \frac{L_i}{f} \tag{26}$$

$$L_i = L_{i-1} + \frac{W_{Mi}}{2} \left[\frac{-\sin \beta_i}{\cot \theta_{t_0}} + \cos \beta_i \right] + \frac{W_{Mi-1}}{2} \left[\frac{-\sin \beta_{i-1}}{\cot \theta_{t_0}} + \cos \beta_{i-1} \right] \tag{27}$$

$$W_{Mi} \cdot [\cos(\beta_i + \theta_{t_0}) - \sin(\beta_i + \theta_{t_0}) \tan \alpha_i] = W_{PV} \tag{28}$$

Given its particular structure, this system has to be solved progressively, from $i = 1$ to $i = n$, starting with the values computed for $i = 0$.

1. 4. Increase θ_{t_0} by the discretization and repeat the above steps, until $\theta_{t_0} > M$.

Notice that before starting, we need to compute T using Equation (2):

$$\theta_t = F(N, T) \Rightarrow T = h(N, \theta_t) \tag{29}$$

in order to define $h(N, \theta_t)$ implicitly. If we particularize θ_t to $\pm\theta_{t_0}$, we obtain two (implicitly defined) functions $h_R(N, \theta_{t_0})$ and $h_S(N, \theta_{t_0})$:

$$-\theta_{t_0} = F(N, T) \Rightarrow T = h_R(N, \theta_{t_0}) \tag{30}$$

$$\theta_{t_0} = F(N, T) \Rightarrow T = h_S(N, \theta_{t_0}) \tag{31}$$

symmetrical with respect to $T = 12$ (so that we only need to solve one of them). The R and S as subindices come from “sunRise” and “sunSet”, although, properly speaking, they indicate the time at which the system should start and stop operating, respectively. We shall, nevertheless, speak of sunrise and sunset functions, when referring to them. We can now define the optimum operating interval as a function of T :

$$T \in I_N = [h_R(N, \theta_{t_0}), h_S(N, \theta_{t_0})] \tag{32}$$

which depends, certainly, on the day of the year N .

4.3. Influence of θ_{t_0} on the total irradiation received

We use the method proposed in Ref. [33] to determine the hourly distribution of beam horizontal solar irradiance for each day of the year, $I_{bh}(N, T)$. That study demonstrates the accuracy of the method and its applicability to different climates, checking against real data obtained from ground-level stations (for instance, from the WRDC database). By means of the Fourier transform, it obtains good estimations of the beam and diffuse solar irradiations for each day of the year. The authors use the Hottel clear-skies model [36] and data from the PVGIS database [37].

In the previous step, we specified a design angle θ_{t_0} which (as the forthcoming examples will show) has a large direct bearing on the width of the SSLFR. Now we study its influence on the solar irradiation received by the PV cells. To this end, we are going to integrate, for each day N and for each θ_{t_0} , the irradiation absorbed throughout the interval (32) (obviously, this depends on the location):

$$\tilde{H}_{bh}(N, \theta_{t_0}) = \int_{h_R(N, \theta_{t_0})}^{h_S(N, \theta_{t_0})} I_{bh}(N, T) dT \tag{33}$$

In that interval, we know for sure that there is neither shading nor blocking. We are going to compare $\tilde{H}_{bh}(N, \theta_{t_0})$ with the total irradiance from true sunrise ($T_R(N)$) to true sunset ($T_S(N)$):

$$H_{bh}(N) = \int_{T_R(N)}^{T_S(N)} I_{bh}(N, T) dT \tag{34}$$

Notice, however, that it would be impossible to prevent blocking and shading during the whole interval $[T_R(N), T_S(N)]$ (for instance, the solar height at both times is 0). Thus, the value of $H_{bh}(N)$ is just the an upper bound for the absorbed irradiations and one must be aware of this fact during the design process. The combination of the two elements:

1. The width of the SSLFR

$$W = 2L_n + W_{Mn} \tag{35}$$

2. The ratio of yearly absorbed irradiation:

$$P_{\tilde{H}} = \sum_{N=1}^{365} \tilde{H}_{bh}(N, \theta_{t_0}) / \sum_{N=1}^{365} H_{bh}(N) \tag{36}$$

will be the key tools for the designer with which to choose his or her optimal θ_{t_0} , depending on other constraints (technical, economic, geographical ...).

5. Analysis of the proposed design of the SSLFR

Once the design phase has been finished, with θ_{t_0} chosen and the optimal values of the number n of mirrors, their positions L_i and their widths W_{Mi} are fixed, we study the behavior of the SSLFR applied to PV generation. Recall that the tilt of the mirrors follows the transverse angle θ_t with the formula:

$$\beta_i = \frac{-\theta_t \pm \alpha_i}{2}, \quad 1 \leq i \leq n \tag{37}$$

Recall also that our SSLFR has been designed for an optimal performance for $T \in I_N$ (see (32)), and this interval is differs between days. We now study three relevant aspects: the dimensions of the cooling system, the equations governing blocking and shading out of the optimum operation interval, and finally, how to compute the active power of the PV system.

The following property is easily verified.

Property 2. For any θ_t , and any mirror i , the value $W_{fi}(N, T, i)$ is constant as long as T is given by the implicit function $h(N, \theta_t)$.

Property 2 is easily understood: once all the positions of the mirrors are fixed (all the α_i), the value of W_{fi} depends only on θ_t . From this property follows that, for instance, at (the systems’) sunrise and sunset $h_R(N, \theta_{t_0})$, $h_S(N, \theta_{t_0})$, the width W_{fi} is the same every day. The difference is that it is reached at different times each day.

Another property (which we shall use later on in this section) is that the maximum value of W_{fi} for each mirror i is independent of the day N (although, again, it is reached at different times). Once this maximum value is known, we shall verify that the PV cells are always receiving solar irradiance, and we shall be able to compute the input power.

5.1. Shading and blocking out of the optimum operation interval

In the previous section, the SSLFR was designed so that during the working interval

$$\theta_t \in [-\theta_{t_0}, \theta_{t_0}] \tag{38}$$

there was neither shading nor blocking between adjacent mirrors. We now study what happens when θ_t is out of this interval. As above, we only provide the explicit calculations for the mirrors on the left side.

Let s_i be the distance between two adjacent mirrors (mirror $i - 1$ and i), in the optimal design for $\theta_t = \theta_{t_0}$. From (10) and (11) follows that:

$$s_i = L_i - L_{i-1} = \frac{W_{Mi}}{2} \left[\frac{-\sin \beta_i}{\cot \theta_{t_0}} + \cos \beta_i \right] + \frac{W_{Mi-1}}{2} \left[\frac{-\sin \beta_{i-1}}{\cot \theta_{t_0}} + \cos \beta_{i-1} \right] \tag{39}$$

with:

$$\beta_i = \frac{-\theta_{t_0}}{2} - \frac{1}{2} \arctan \frac{L_i}{f} \tag{40}$$

Let s_i^* be the value obtained for a general θ_t :

$$s_i^* = \frac{W_{Mi}}{2} \left[\frac{-\sin \beta_i}{\cot \theta_t} + \cos \beta_i \right] + \frac{W_{Mi-1}}{2} \left[\frac{-\sin \beta_{i-1}}{\cot \theta_t} + \cos \beta_{i-1} \right] \tag{41}$$

with:

$$\beta_i = \frac{-\theta_t}{2} - \frac{1}{2} \arctan \frac{L_i}{f} \tag{42}$$

The simplest way to check whether there is shading or not is the following test:

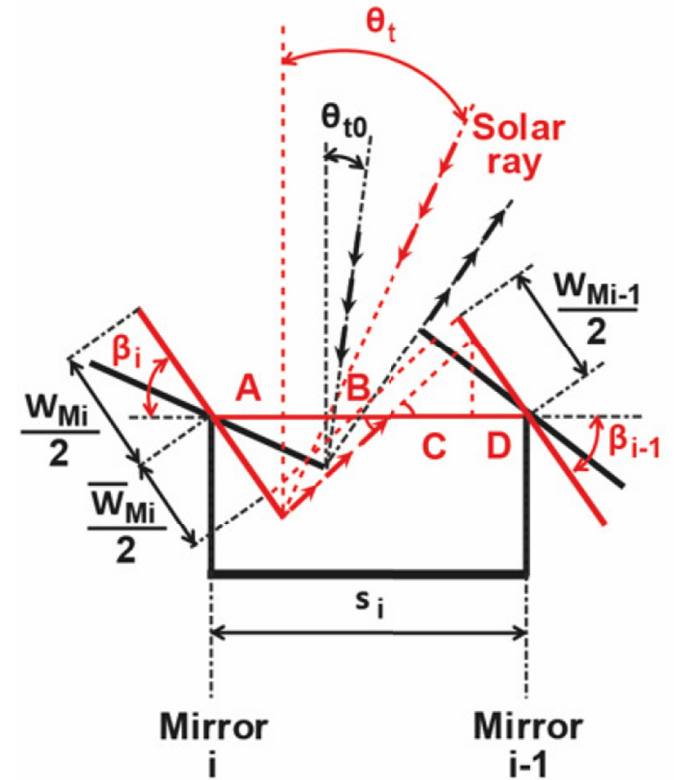


Fig. 13. Computing the blocking.

$$\begin{aligned} \text{If } s_i^* \leq s_i &\rightarrow \text{No shading} \\ \text{If } s_i^* > s_i &\rightarrow \text{Shading} \end{aligned} \tag{43}$$

Assuming now that there is shading (i.e. $s_i^* > s_i$), let us compute its magnitude. From Fig. 12, for two consecutive mirrors on the left side:

$$s_i = A + B + C + D = \frac{\overline{W}_{Mi}}{2} \left[\frac{-\sin \beta_i}{\cot \theta_t} + \cos \beta_i \right] + \frac{W_{Mi-1}}{2} \left[\frac{-\sin \beta_{i-1}}{\cot \theta_t} + \cos \beta_{i-1} \right] \tag{44}$$

where the width of the mirror causing the shading is:

$$\frac{W_{Mi}}{2} + \overline{W}_{Mi} = \frac{W_{Mi}}{2} + \frac{s_i - \frac{W_{Mi-1}}{2} \left[\frac{-\sin \beta_{i-1}}{\cot \theta_t} + \cos \beta_{i-1} \right]}{\left[\frac{-\sin \beta_i}{\cot \theta_t} + \cos \beta_i \right]} \tag{45}$$

In this formula, \overline{W}_{Mi} can be either positive or negative. As regards blocking, reasoning analogously using Fig. 13, the width of the mirror free of blocking is:

$$\frac{W_{Mi}}{2} + \overline{W}_{Mi} = \frac{W_{Mi}}{2} + \frac{s_i - \frac{W_{Mi-1}}{2} \left[\frac{-\sin \beta_{i-1}}{\cot \alpha_i} + \cos \beta_{i-1} \right]}{\left[\frac{-\sin \beta_i}{\cot \alpha_i} + \cos \beta_i \right]} \tag{46}$$

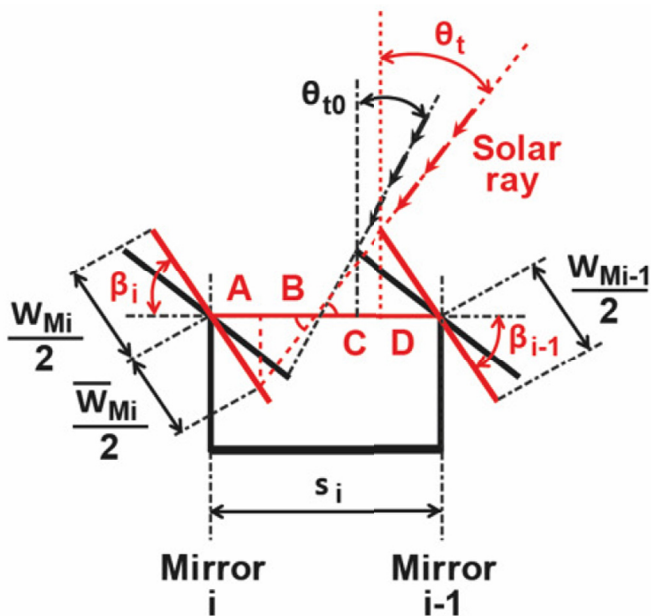


Fig. 12. Computing the shading.

5.2. Power reaching on the PV cells

The power reaching the PV cells can be calculated using the following formula proposed by Morin [27]:

$$Q = DNI \cdot \eta_{opt} \cdot IAM \cdot A_{eff} \cdot \eta_{endloss} \quad (47)$$

where DNI is the direct normal irradiance (W/m^2), η_{opt} the optical efficiency of the SSLFR, A_{eff} the total effective mirror area (m^2), $\eta_{endloss}$ the end loss efficiency, which relates to the area of the receiver which is not illuminated by the reflected rays in the longitudinal study, and finally IAM is the incidence angle modifier, a coefficient which includes shading and blocking of reflected rays and an incidence cosine for each mirror element. This IAM is often divided into its transverse and longitudinal components as:

$$IAM = IAM_T(\theta_t) \cdot IAM_L(\theta_l) \quad (48)$$

As the configuration chosen in the longitudinal study satisfies the condition:

$$\beta_M = \beta_S = \theta_z/2 \quad (49)$$

we can conclude that all the length L_{PV} is uniformly illuminated, and that:

$$\eta_{endloss} = 1; \theta_l = \theta_z/2 \quad (50)$$

In order to compute A_{eff} , we need to consider several factors. We have already guaranteed that the effectively illuminated length is all of L_{PV} . We also need to know the width W_{fi} (the width really illuminated); during the optimum operation time I_N , the equality $\min\{W_{fi}, W_{PV}\} = W_{PV}$ holds, but we need to compute the value of that minimum out of that interval (for some mirrors, it will be W_{fi} instead of W_{PV}). Finally, a shading and blocking factor F_{bs} must be included, whose value is 1 during the operating interval I_N (there is none of either), and which is computed using Formulas (45) and (46) at other times. After all these elements are taken into account, we suggest (as a consequence of the Principle of Conservation of Energy) the following formula for the power reaching the PV cells:

$$Q = \sum_{i=1}^{2 \cdot n + 1} DNI \cdot \eta_{opt} \cdot L_{PV} \cdot \min\{W_{fi}, W_{PV}\} \cdot F_{bs} \cdot \cos \theta_i \cdot \cos \theta_l \quad (51)$$

Where the transverse angle θ_i between the normal to the i -th mirror and the incidence angle of the Sun satisfies (and can be computed from):

$$\cos \theta_i = \cos(\beta_i \pm \alpha_i)$$

with + for the left side, and – for the right side of the SSLFR.

6. Numerical results and verification

In order to provide a better explanation of our method, we show in what follows the results obtained at a location in Almería (Spain), whose geographical data are: latitude $36^\circ 50' 07'' N$, longitude $02^\circ 24' 08'' W$ and elevation 22 (m).

In Table 2 we include the fixed parameters of the SSLFR considered for simulation and verification.

The configuration chosen in the longitudinal study allows us to take $L_{PV} = L_M$. From the point of view of optical design, the materials of interest are: mirror, and glass of the PV cells. Their optical properties and the cleanliness factor of the SSLFR ([25,34,35]) are contained in Table 1.

All the optical properties can be gathered together in what is known as the total optical yield (η_{opt}):

$$\eta_{opt} = \rho \cdot CL_m \cdot CL_g \cdot \tau_g \quad (52)$$

where ρ is the reflectivity of the mirrors, CL_m is their cleanliness factor, CL_g is the cleanliness factor of the glass, τ_g is its transmissivity. All these parameters are dimensionless.

6.1. Optimal design of the SSLFR

In order to find the optimal design, it is convenient to choose $m = 30^\circ$ and $M = 60^\circ$ as the endpoints for θ_{t_0} . All our computations have been made using Mathematica 10™. We first compute the functions $h_R(N, \theta_{t_0})$ and $h_S(N, \theta_{t_0})$ just solving for each N and $\theta_{t_0} \in [m, M]$ the equation:

$$\theta_t(N, T) = \pm \theta_{t_0} \quad (53)$$

The number of hours with a guaranteed homogeneous distribution of solar irradiance, with neither shading nor blocking (i.e. the length of the operation interval $[h_R(N, \theta_{t_0}), h_S(N, \theta_{t_0})]$) is given in Fig. 14, for $\theta_{t_0} \in [m, M]$ in intervals of 5° .

We have carried out several simulations for different values of n , using the iterative algorithm. For $n = 2$, the values obtained for the width of the SSLFR allow a greater variation of θ_{t_0} in the design. Hence we choose this value for n , the first parameter of the design.

Now the method computes the optimum width for each value of $\theta_{t_0} \in [m, M]$ (see Fig. 15). It gives a convex function (this was easy to guess) with a large derivative for the largest values of θ_{t_0} .

Once the strictly geometrical study of the SSLFR has been performed, we deal with the second key element for its design: Fig. 16

Table 2
Fixed parameters of the SSLFR.

	Parameters	Value
W_{PV}	PV system width	0.28 (m)
L_{PV}	PV system length	2.00 (m)
W_{ACS}	Cooling system width	0.30 (m)
L_{ACS}	Cooling system length	2.00 (m)
f	Height of the receiver	1.50 (m)
L_M	Mirror length	2.00 (m)
ρ	Mirror reflectivity	0.94
CL_m	Mirror cleanliness	0.96
CL_g	Glass cleanliness	0.96
τ_g	Glass transmissivity	0.92

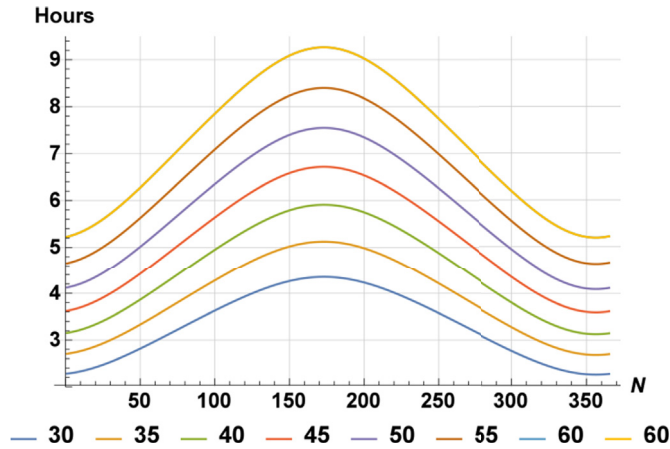


Fig. 14. Hours of optimum operation.

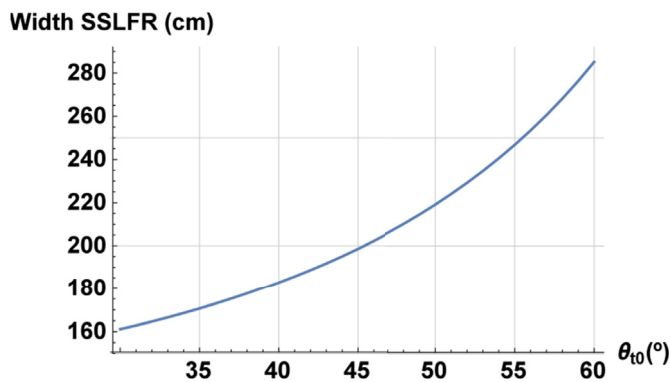


Fig. 15. Width SSLFR vs. θ_{t_0} .

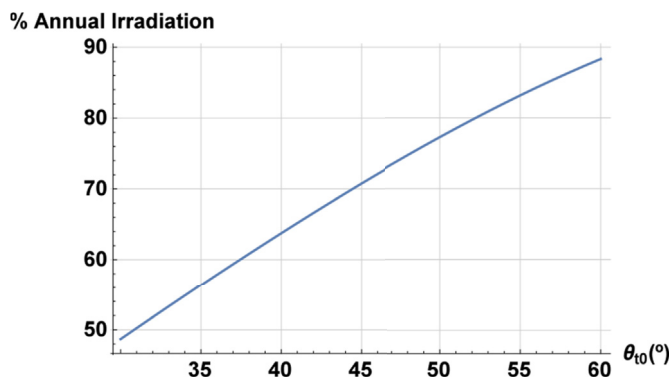


Fig. 16. Annual irradiation vs. θ_{t_0} .

depicts the variation of the % of annual irradiation which effectively reaches the PV system (which we usually denote P_{H1}), as a function of θ_{t_0} .

Finally, in order to make the final design decision, in Fig. 17 the width of the SSLFR is plotted against the % of total annual solar irradiation effectively reaching the PV cells. This is the “compromise” curve between two opposed objectives to be optimized (the

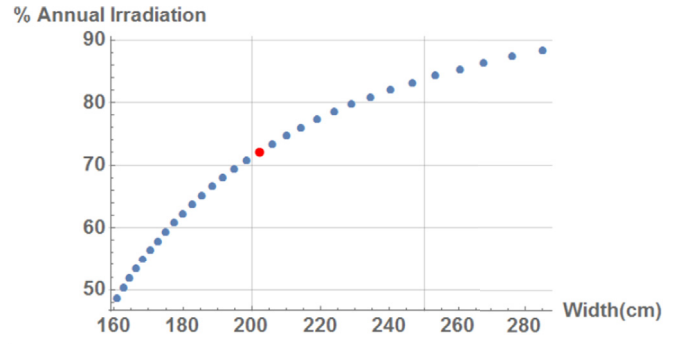


Fig. 17. Width vs. irradiation.

Table 3
Geometric values of the optimal design.

Mirror	L_i (cm)	W_{Mi} (cm)	max W_{fi} (cm)
1	85.7181	30.7973	35.4712
2	41.9636	31.3971	32.6025
3	0.00	30.4181	30.4181
4	41.9636	31.3971	32.6025
5	85.7181	30.7973	35.4712

Pareto optimum front), in our case the most important curve for the design. We have chosen a discretization of 1° for the interval $\theta_{t_0} \in [m, M]$, so that each point represents an integer value of θ_{t_0} . Using that plot, we have decided to choose $\theta_{t_0} = 46^\circ$ (marked on the plot). This decision is based on two reasons: we were loath to have a width much larger than 200 (cm) (and the chosen point gives 203 (cm)); furthermore, it guarantees receiving 72.19% of the unreachable ideal value of 100% yearly irradiation, which we deem good enough.

Table 3 contains the geometric values of L_i and W_{Mi} for this optimal design. At this point, we number the mirrors from left to right starting at 1. As there are 5 mirrors, the central one is number 3. Apart from the obvious symmetry, we point out that the distances d_i between mirrors vary between 11.06 (from the central one to its adjacent one) and 12.66 (from the two extremal ones to their adjacent ones).

Another interesting feature is what we call the occupation factor of the primary field: the quotient between the total true surface of the mirrors A_M (not counting their distances) over the total surface of the reflector area: A_R :

$$F_{MR} = \frac{A_M}{A_R} \tag{54}$$

In this design we get $F_{MR} = 0.77$. This value is important when computing the concentration of the SSLFR and the suns actually reaching the PV cells.

The third column of Table 3 contains the maximum values of W_{fi} for each mirror. As we saw in Property 2, this maximum is independent of the day number but depends on the time of the day (except for the central mirror, for which it happens at noon). This value lets us quantify the discarded radiation in the worst circumstances. Although our present design does not take it into account, it is also a good tool when a secondary concentrator is involved.

Table 4
Unused mirror surface (%) due to shading, $N = 172$.

n \ T	6.56	7.16	7.77	8.37	I_{172}	15.63	16.23	16.84	17.44
1	44.64	30.03	16.41	3.72	0.	0.	0.	0.	0.
2	41.40	27.56	14.89	3.33	0.	0.	0.	10.56	26.02
3	36.67	22.03	8.96	0.	0.	0.	8.96	22.03	36.67
4	26.02	10.56	0.	0.	0.	3.33	14.89	27.56	41.40
5	0.	0.	0.	0.	0.	3.72	16.41	30.03	44.64

Regarding the calculation of shading and blocking outside the optimum operation interval, we only include two cases, for the sake of brevity: the summer and winter solstices ($N = 172$ and $N = 355$, respectively). For the summer solstice, the optimum operation interval for $\theta_{t_0} = 46^\circ$ is $T \in I_{172} = [8.56, 15.44]$ (approx. 7 h). During that interval, we know there is neither shading nor blocking.

Table 4 shows the % of unused surface for each mirror (at different times) when the operation time is extended 2 h on each end, for $N = 172$. This value is directly related to the % of lost power and, as can be seen reaches values near 45% on the extremal mirrors (the ones on the right in the early morning, the ones on the left in the late afternoon). Notice the totally symmetrical operation of the SSLFR. This analysis helps us realize the importance of the previous

Table 5
Unused mirror surface (%) due to shading, $N = 355$.

n \ T	8.15	8.58	9.01	9.44	9.86	I_{355}	14.14	14.56	14.99	15.42	15.85
1	67.30	53.07	38.72	24.25	9.74	0.	0.	0.	0.	0.	0.
2	63.37	49.50	35.76	22.14	8.79	0.	0.	4.74	19.62	35.44	52.19
3	60.59	45.39	30.66	16.40	2.78	0.	2.78	16.40	30.66	45.39	60.59
4	52.19	35.44	19.62	4.74	0.	0.	8.79	22.14	35.76	49.50	63.37
5	0.	0.	0.	0.	0.	0.	9.74	24.25	38.72	53.07	67.30

phases of the design which prevent us from losing too much irradiation during operation.

Table 5 shows the same statistics for $N = 355$, for which the optimum operation time for $\theta_{t_0} = 46^\circ$ is $T \in I_{355} = [10.15, 13.85]$ (around 3 h 45 m). The results are much more striking and losses accrue up to more than 66%.

Finally, we provide the input power on the PV cells, for the same days as before: $N = 172$, and $N = 355$ (both solstices), using (51) to compute it. Figs. 18 and 19 show the plot of Q for those days throughout the operating interval I_N (the vertical lines) and out of it. Notice the blunt change of shape of the curve at the endpoints of I_N due to the apparition of shading and blocking (F_{bs} takes values less than 1 there), i.e. the loss of useful mirror surface. This parallels the data in Tables 4 and 5, obviously. That effect is also caused by the fact that $\min\{W_{fi}, W_{pv}\}$ can be W_{fi} instead of W_{pv} outside I_N . Notice how the increase of Q outside the operating interval is greater for day $N = 355$ than for $N = 172$. This is due to the greater influence of shading in the Winter days than in the Summer.

A useful value for evaluating non-optimal configurations with respect to the best one is the *energy gain reduction*. Non-optimal configurations, apart from possibly producing non-uniform illumination on the PV cells, also incur energy gain reduction. This is computed as the relative difference (in %) between the energies

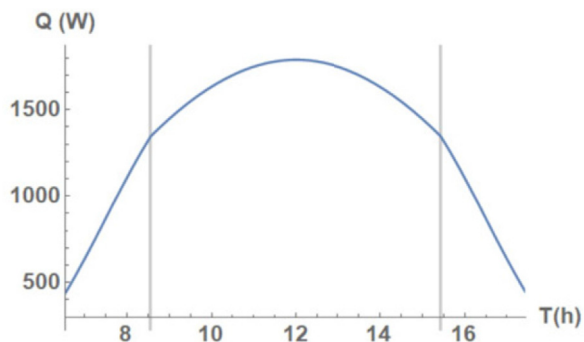


Fig. 18. Power for $N = 172$.

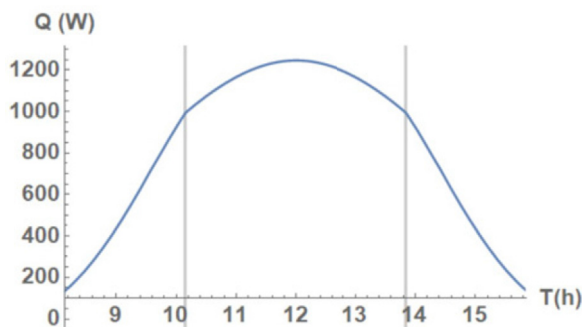


Fig. 19. Power for $N = 355$.

absorbed by the non-optimal and the optimal configurations:

$$EGR = \frac{E_{Non-optimal} - E_{Optimal}}{E_{Optimal}} \cdot 100 \tag{55}$$

Table 6
Parameters of the non-optimal configurations.

Conf.	Causes of non-uniform illumination	d (m)	n	W_M (m)	W_{PV} (m)
1	Shading and blocking contribution to non-uniformity (small d)	0.05	2	0.30	0.28
2	Separation between mirrors (small d)	0.08	2	0.30	0.28
3	Separation between mirrors (small d)	0.10	2	0.30	0.28
4	Separation between mirrors (large d)	0.12	2	0.30	0.28
5	Separation between mirrors (large d)	0.14	2	0.30	0.28

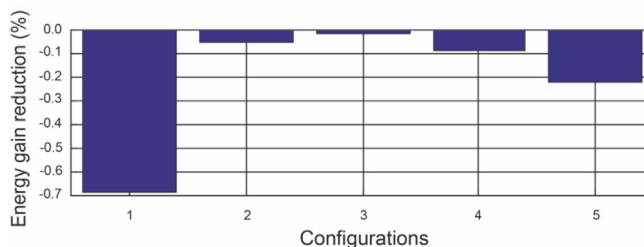


Fig. 20. Annual energy gain reduction for non-optimal configurations vs. optimal configuration.

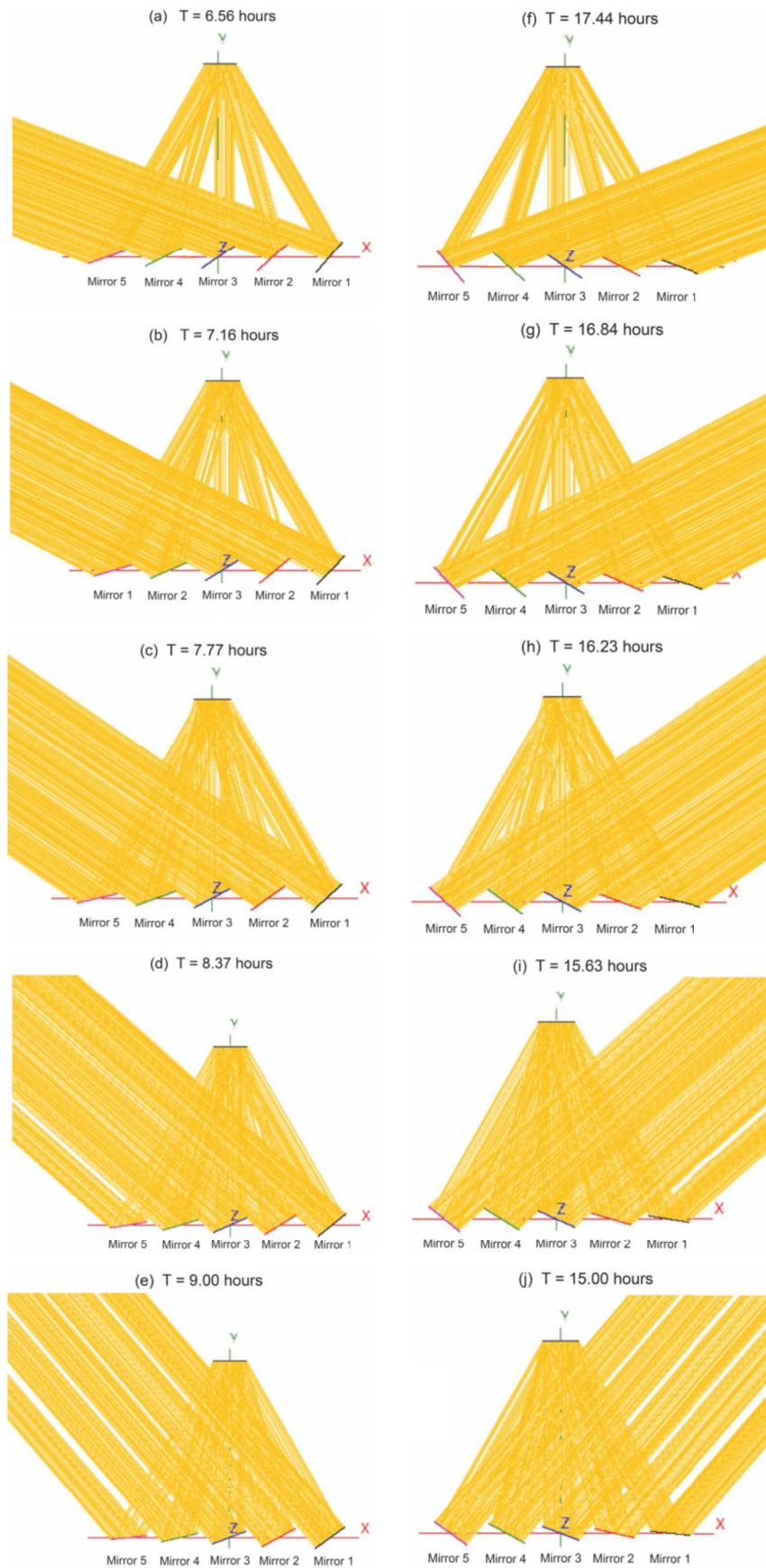


Fig. 21. SolTrace 2D view of SSLFR for $N = 172$.

Table 7
Unused mirror surface (%) due to shading with SolTrace, $N = 172$.

n \ T	6.56	7.16	7.77	8.37	I_{172}	15.63	16.23	16.84	17.44
1	44.25	29.71	16.07	3.40	0.	0.	0.	0.	0.
2	41.08	27.16	14.51	2.93	0.	0.	0.	10.18	25.63
3	36.29	21.66	8.58	0.	0.	0.	8.58	21.66	36.29
4	25.63	10.18	0.	0.	0.	2.93	14.51	27.16	41.080
5	0.	0.	0.	0.	0.	3.40	16.07	29.71	44.25

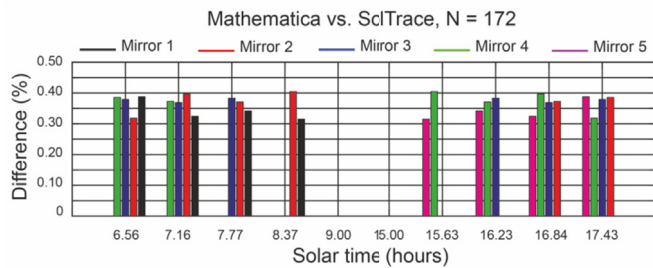


Fig. 22. Difference of unused surface with Mathematica vs. SolTrace.

Table 6 shows the parameters in the non-optimal configurations we have studied, whereas in Fig. 20 we have plotted the yearly energy gain reduction, with respect to our optimal configuration. The most notable losses happen for the shading and blocking and, generally the larger the (non-optimal) distance between mirrors, the greater the losses, as well. Notice how the parameters of Configuration 3 are practically equal to the optimal one (however, one must take into account that in the optimal configuration, the distances between mirrors are not constant).

6.2. Verification by Monte Carlo simulation

We verify our computations showcasing a simulation using Monte Carlo Ray Tracing method, with SolTrace™. In order to carry it out, a 3D model of the optimal design of the SSLFR has to be provided to the software (following the data in Table 4). All the mirrors are assumed flat, perfect, and their reflectivity a cleanliness are given in Table 3, as are for the receiver surface. We choose 10^7 rays for the simulation and the direct normal irradiance for each day of the year follows [33].

Fig. 21 is a snapshot of the output of SolTrace for the Summer Equinox $N = 172$ (see Table 4). The first four plots (Fig. 21(a)–21(d)) correspond to times outside the optimum operation interval, before noon: there is noticeable shading on the central and west-side mirrors (1, 2 and 3). Fig. 21(f)–21(i) are for times also outside the optimum operation interval, but after noon: the shading happens on the central and east-side mirrors (3, 4 and 5). Finally, Fig. 21(e) and (j) correspond to times inside the optimum operation interval: there is no shading.

Table 7 contains the % of unused mirror area given by Soltrace, and Fig. 22 is the graphical relative comparison between the Mathematica model and the Soltrace simulation for $N = 172$ (the Summer Solstice), which shows the practical equality between both models (0.04% at most, in relative terms).

The flux density on the PV cells for $N = 172$ obtained with

SolTrace is provided in Fig. 23. Fig. 23(a)–23(d) correspond to times outside the optimum operation interval before noon. Notice how for $T = 6.56$ (Fig. 23(a)) there is very low or null flux density on the east side due to the shading of the mirrors on the west side (as seen in Fig. 21), and that W_{fi} (the transversely illuminated length) is less than 0.28 (the width of the PV cells). This negative effects decrease as T approaches noon. A parallel process can be seen in Fig. 23 (f)–23(i), for the east side, after noon. Finally, in Fig. 23(e) and (j), we show two times inside the optimum operation interval, where the flux density is totally homogeneous on the PV cells.

Table 8 shows three flux densities on the PV cells: the one coming from the DNI, the one given by the SolarTrace simulation, and the theoretical one, obtained with our procedure, as another verification point.

7. Conclusions and future perspectives

We have analyzed the main causes of non-uniform illumination of the photovoltaic cells in low concentration photovoltaic systems based on small-scale linear Fresnel reflectors in order to optimize the design of such a reflector with respect to PV power generation, as heterogeneity in the distribution of the reflected solar irradiance decreases the efficiency of the photovoltaic cells. To prevent this issue, we define an optimum operation interval which ensures that the distribution of reflected rays on the PV cells is homogeneous and that there is neither shading nor blocking on the mirrors. This interval is defined in terms of the extremal transverse incidence angle θ_{t_0} , which is computed using Mathematica™. We show the influence of θ_{t_0} on the main parameters of the SSLFR: mirror widths, number of mirrors and their positions. We carry out a transverse and longitudinal study of the SSLFR, the effect of θ_{t_0} on other factors like the time span of the optimum operation interval, the total annual solar irradiation absorbed by the system, the width of the mirrors and their positions. We include a full simulation using Monte Carlo Ray Tracing method in order to verify our equations. In this simulation, the shading effects are patent for times outside the optimum operation time. The simulation also provides a graphical verification of our equations, differing less than 2.2% in the predicted flux density on the PV cells.

The main conclusions from our analysis are:

1. The required width of the SSLFR with respect to θ_{t_0} is a convex function with a large derivative for great values of θ_{t_0} .
2. There is a trade-off between the width of the SSLFR (which should not be large) and the total annual absorbed irradiation, depending on θ_{t_0} , and the designer has to decide where to set the optimum value.
3. The optimum number of mirrors for the specified receiver height of 150 (cm) provided by our method is actually 5. The value of θ_{t_0} for which the annual irradiation is maximum (for a total field width of 203 (cm)) is 46° , for which the ratio of absorbed irradiation with respect to the theoretical maximum is 72%.

Future work will entail the study of the performance of the proposed system in terms of both thermal and electrical efficiency, and a cost-benefit analysis.

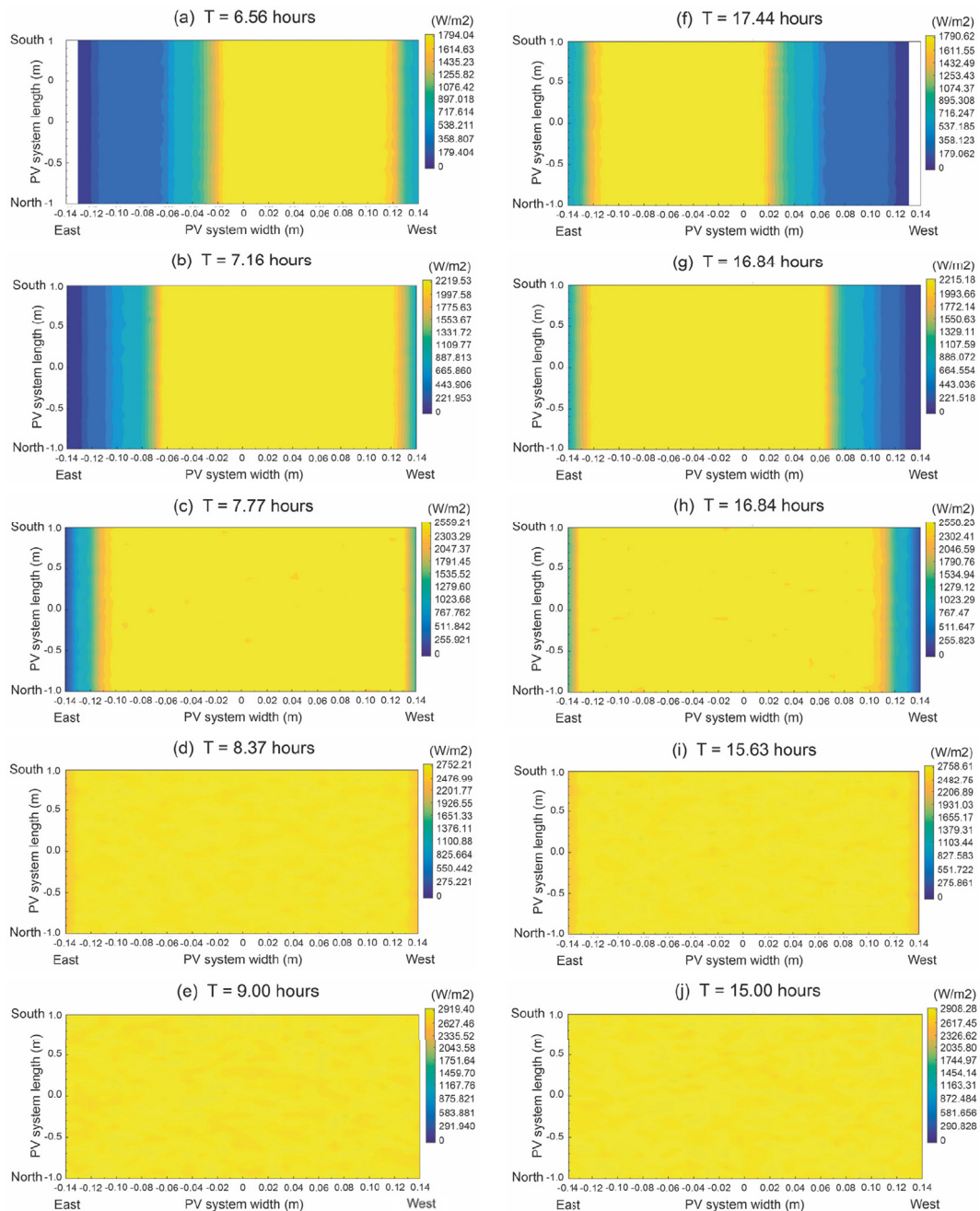


Fig. 23. SolTrace 2D view of flux density in PV cells for $N = 172$.

Table 8
Comparison of flux density (model and SolTrace simulation).

T	DNI (W/m^2)	SolTrace (W/m^2)	Mathematica (W/m^2)	Diff. (%)
6.56	481.00	808.08	790.76	2.18
7.16	582.17	1293.82	1267.67	2.06
7.77	656.53	1817.14	1781.98	1.97
8.37	709.65	2302.25	2264.94	1.64
9.00	750.19	2620.87	2583.89	1.43
15.00	750.19	2620.91	2583.89	1.43
15.63	709.65	2302.19	2264.94	1.64
16.23	656.53	1817.14	1781.98	1.97
16.84	582.17	1293.86	1267.67	2.06
17.44	481.00	808.05	790.76	2.18

Credit author statement

A. Barbón: Conceptualization, Methodology. **P. Fortuny Ayuso:** Software, Methodology, Writing – original draft preparation. **L. Bayón:** Conceptualization, Methodology. **J. A. Fernández-Rubiera:** Software, Conceptualization, Methodology.

Declaration of competing interest

The authors declare that they have no known competing financial interests or personal relationships that could have appeared to influence the work reported in this paper.

Acknowledgments

We wish to thank Dr. Laudino Rodríguez, head of the CIPP-Mantenimiento y Servicios a la Producción vocational training school in La Felguera, Asturias, Spain, for their work building of the prototype for the design presented in this paper.

References

- [1] Yilmaz S, Ozcalik HR, Kesler S, Dincer F, Yelmen B. The analysis of different PV power systems for the determination of optimal PV panels and system installation—a case study in Kahramanmaraş, Turkey. *Renew Sustain Energy Rev* 2015;52:1015–24.
- [2] Jacobson MZ, Delucchi MA, Bauer ZAF, Goodman SC, Chapman WE, Cameron MA, Bozonnat C, Chobadi L, Clonts HA, Enevoldsen P, Erwin JR, Fobi SN, Goldstrom OK, Hennessy EM, Liu J, Lo J, Meyer CB, Morris SB, Moy KR, O'Neill PL, Petkov I, Redfern S, Schucker R, Sontag MA, Wang J, Weiner E, Yachanin AS. 100% clean and renewable wind, water, and sunlight (WWS) all-sector energy roadmaps for 139 countries of the world. *Joule* 2017;1:108–21 [Alphabetical].
- [3] IRENA. Future of solar photovoltaic: deployment, investment, technology, grid integration and socio-economic aspects. International Renewable Energy Agency; 2019. Available at: https://irena.org/-/media/Files/IRENA/Agency/Publication/2019/Nov/IRENA_Future_of_Solar_PV_2019.pdf.
- [4] Alzahrani M, Shanks K, Mallick TK. Advances and limitations of increasing solar irradiance for concentrating photovoltaics thermal system. *Renew Sustain Energy Rev* 2021;138:110517.
- [5] Amanlou Y, Tavakoli Hashjin T, Ghobadian B, Najafi G, Mamat R. A comprehensive review of uniform solar illumination at low concentration photovoltaic (LCPV) systems. *Renew Sustain Energy Rev* 2016;60:1430–41.
- [6] Tripathi B, Yadav P, Lokhande M, Kumar M. Feasibility study of commercial silicon solar PV module based low concentration photovoltaic system. *Int J Electr Electron Eng Res* 2012;2(3):84–93.
- [7] Wang G, Shen F, Wang F, Chen Z. Design and experimental study of a solar CPV system using CLFR concentrator. *Sustain Energy Technol Assess* 2020;40:100751. 2020.
- [8] Wang G, Wang F, Shen F, Jiang T, Chen Z, Hu P. Experimental and optical performances of a solar CPV device using a linear Fresnel reflector concentrator. *Renew Energy* 2020;146:2351–61.
- [9] Liu Y, Hu P, Zhang Q, Chen Z. Thermodynamic and optical analysis for a CPV/T hybrid system with beam splitter and fully tracked linear Fresnel reflector concentrator utilizing sloped panels. *Sol Energy* 2014;103:191–9.
- [10] Ghodbane M, Evangelos Bellos E, Said Z, Boumeddane B, Kadhim Hussein A, Kolsi L. Evaluating energy efficiency and economic effect of heat transfer in copper tube for small solar linear Fresnel reflector. *J Therm Anal Calorim* 2021;143:4197–215.
- [11] Barbón A, Sánchez-Rodríguez JA, Bayón L, Bayón-Cueli C. Cost estimation relationships of a small scale linear Fresnel reflector. *Renew Energy* 2019;134:1273–84.
- [12] Baig H, Heasman KC, Mallick TK. Non-uniform illumination in concentrating solar cells. *Renewable Sustain Energy Reviews* 2012;16:5890–5909.
- [13] Or AB, Appelbaum J. Performance analysis of concentrator photovoltaic dense-arrays under non-uniform irradiance. *Sol Energy Mater Sol Cells* 2013;117:110–9.
- [14] Guerriero P, Tricoli P, Daliento S. A bypass circuit for avoiding the hot spot in PV modules. *Sol Energy* 2019;181:430–8.
- [15] He Y-L, Zhou Y-P, Hu Y-H, Hung T-C. A multiscale-multiphysics integrated model to investigate the coupling effects of non-uniform illumination on concentrated photovoltaic system with nanostructured front surface. *Appl Energy* 2020;257:113971.
- [16] Fernández A, Laguna G, Rosell J, Vilarrubí M, Ibañez M, Sisó G, Illa J, Barrau J. Assessment of the impact of non-uniform illumination and temperature profiles on a dense array CPV receiver performance. *Sol Energy* 2018;171:863–70.
- [17] Michael JJ, Iqbal SM, Iniyar S, Goic R. Enhanced electrical performance in a solar photovoltaic module using V-trough concentrators. *Energy* 2018;148:605–13.
- [18] Li G, Xuan Q, Pei G, Su Y, Ji J. Effect of non-uniform illumination and temperature distribution on concentrating solar cell – a review. *Energy* 2018;144:1119–36.
- [19] Sánchez-González A, Gómez-Hernández J. Beam-down linear Fresnel reflector: BDLFR. *Renew Energy* 2020;146:802–15.
- [20] Wendelin T, Dobos A, Lewandowski A. Tech. Rep., in: SolTrace: a ray-tracing code for complex solar optical systems, NREL. Golden, Colorado: National Renewable Energy Laboratory; 2013. Available on line at, <http://www.nrel.gov/docs/fy14osti/59163.pdf>.
- [21] Barbón A, Barbón N, Bayón L, Otero JA. Theoretical elements for the design of a small-scale linear fresnel reflector: frontal and lateral views. *Sol Energy* 2016;132:188–202.
- [22] Barbón A, Bayón L, Bayón-Cueli C, Barbón N. A study of the effect of the longitudinal movement on the performance of small scale linear Fresnel reflectors. *Renew Energy* 2019;138:128–38.
- [23] Ghodbane M, Boussad B, Noureddine S. A linear Fresnel reflector as a solar system for heating water: theoretical and experimental study. *Case Stud Therm Eng* 2016;8:176–86.
- [24] Bermejo P, Pino FJ, Rosa F. Solar absorption cooling plant in Seville. *Sol Energy* 2010;84:1503–12.
- [25] Duffie JA, Beckman WA. Solar engineering of thermal processes. John Wiley & Sons; 2013.
- [26] Barbón A, Fernández-Rubiera JA, Martínez-Valledor L, Pérez-Fernández A, Bayón L. Design and construction of a solar tracking system for small-scale linear Fresnel reflector with three movements. *Appl Energy* 2021;285:116477.
- [27] Morin G, Dersch J, Platzer W, Eck M, Häberle A. Comparison of linear Fresnel and parabolic trough collector power plants. *Sol Energy* 2012;86:1–12.
- [28] Hongn M, Flores Larsen S. Hydrothermal model for small-scale linear Fresnel absorbers with nonuniform stepwise solar distribution. *Appl Energy* 2018;223:329–46.
- [29] Beltagy H. The effect of glass on the receiver and the use of two absorber tubes optical performance of linear fresnel solar concentrators. *Energy* 2021;224:120111.
- [30] Barbón A, Barbón N, Bayón L, Sánchez-Rodríguez JA. Parametric study of the small-scale linear Fresnel reflector. *Renew Energy* 2018;116:64–74.
- [31] Zhu Y, Shi J, Li Y, Wang L, Huang Q, Xu G. Design and thermal performances of a scalable linear Fresnel reflector solar system. *Energy Convers Manag* 2017;146:174–81.
- [32] Zhu Y, Shi J, Li Y, Wang L, Huang Q, Xu G. Design and experimental investigation of a stretched parabolic linear Fresnel reflector collecting system. *Energy Convers Manag* 2016;126:89–98.
- [33] Barbón A, Fortuny Ayuso P, Bayón L, Fernández-Rubiera JA. Predicting beam and diffuse horizontal irradiance using Fourier expansions. *Renew Energy* 2020;154:46–57.
- [34] Sharma VM, Nayak JK, Kedare SB. Effects of shading and blocking in linear Fresnel reflector field. *Sol Energy* 2015;113:114–38.
- [35] Theunissen PH, Beckman WA. Solar transmittance characteristics of evacuated tubular collectors with diffuse back reflectors. *Sol Energy* 1985;35:311–20.
- [36] Hottel HC. A simple model for estimating the transmittance of direct solar radiation through clear atmosphere. *Sol Energy* 1976;18:129–34.
- [37] PVGIS. Joint research centre (JRC). Available on line at, http://re.jrc.ec.europa.eu/pvg_tools/en/tools.html#PVP.